

# Donnan equilibrium effects in protein crystallisation

P. B. Warren

Unilever Research Port Sunlight, Bebington, Wirral, CH63 3JW, United Kingdom

(Dated: 23 January 2002 — PREPRINT)

It is argued that a natural explanation for the scaling collapse of crystallisation boundaries observed for lysozyme [Poon *et al*, J. Phys.: Cond. Mat. **12**, L569 (2000)] can be found by incorporating the idea of a Donnan equilibrium between solution and crystal phases into existing theories for protein phase behaviour. The same theory also explains much of the salt-dependence of the second virial coefficient. The analysis has wider implications for the use of pair potentials to understand protein crystallisation.

PACS numbers: PACS: 64.75.+g, 82.60.Lf, 87.15.Nn

## I. INTRODUCTION

Protein crystallisation is of great practical importance, since high quality crystals are needed for X-ray diffraction work [1]. Under typical conditions where crystals are obtained, the protein-protein interaction appears to be characterised by a hard core repulsion with a strong, short-ranged attraction [2, 3]. For instance, Rosenbaum *et al* [4] successfully collapsed the crystallisation boundaries for a number of proteins onto the adhesive hard sphere (AHS) model [5, 6, 7] by matching the second virial coefficient  $B_2$ . Whilst the AHS model is frequently used to understand protein crystallisation, an important elaboration was introduced by Sear in which crystallisation is the result of a ordering transition driven by sticky patches on the surface of globular proteins [8]. This kind of model may explain the relative difficulty or ease with which different proteins can be crystallised, as discussed below.

Lysozyme is a rather well studied model protein system which readily undergoes crystallisation. The present paper is an attempt to understand some recent observations by Poon *et al* [9] on the scaling collapse of the crystallisation boundary when plotted as a function of  $c_s/Q^2$ , where  $c_s$  is the concentration of NaCl, and  $Q$  the charge on the protein (varied by changing pH [10, 11]). Egelhaaf and Poon also noted a similar scaling collapse for the available literature data for  $B_2$  [12].

Such results are very reminiscent of the Donnan membrane equilibrium, where one finds a contribution to  $B_2$  equal to  $Q^2/4c_s$ , provided that  $c_s \gg Qc_p$  where  $c_p$  is the protein concentration [13]. The effect is well known in polyelectrolyte theory [14]. Donnan's results are usually derived by supposing ideal solution behaviour and imposing electrical neutrality on the two sides of a semi-permeable membrane. It is argued below that the scaling collapse noted by Poon *et al* [9] arises because of an analogous Donnan equilibrium between protein crystals and a dilute protein solution, although in this case there is no semi-permeable membrane and the protein molecules are free to exchange between the two phases.

At first sight this has little to do with the more conventional McMillan-Mayer approach [15, 16] in which effective potentials between proteins are invoked to explain

crystallisation and the effects of added salt, often in the context of DLVO potentials [9] where Debye-Hückel theory is used to account for the charge interactions. However, a close study of the relationship between the two approaches was made by Hill in a series of papers in the 1950s [17]: put succinctly, both the Donnan results and Debye-Hückel theory can be derived from Poisson-Boltzmann theory, using different kinds of approximations. The relationship between these three theoretical approaches is discussed further in the Appendix.

To apply this to the protein crystallisation problem, one needs to incorporate non-ideality of the protein solution, to allow it to form the ordered phase which represents the protein crystals. One therefore needs a 'baseline model' for the freezing transition, to which the Donnan approach can be applied. The first thing to do is to set up this general theory.

## II. GENERAL THEORY

Lysozyme is a charged globular protein of approximate size  $V_p = (\pi/6) \times 4.5 \times 3.0 \times 3.0 \text{ nm}^3 = 21.2 \text{ nm}^3$  [9, 18], or a molar volume  $N_A V_p = 12.8 \text{ M}^{-1}$  where  $N_A$  is Avogadro's number. If the protein concentration is  $c_p$ , the effective volume fraction is  $\phi = V_p c_p$ . The baseline model for the freezing transition referred to above will be fully specified by a dimensionless free energy density  $f^{(0)} = V_p \beta F^{(0)}/V$ , where  $F^{(0)}$  is the free energy of the protein solution or crystal,  $V$  is the system volume, and  $\beta = 1/kT$ . There will be different branches of  $f^{(0)}$  to correspond to the fluid and ordered (crystal) phases. Below I shall consider two possibilities for the baseline model.

The free energy for the full model is obtained from the baseline model by adding in ideal mixing contributions from the coions and counterions (which I suppose to be univalent) and imposing charge neutrality. If the added salt concentration is  $c_s$ , there will be coions at a concentration  $c_s$  and counterions at a concentration  $Qc_p + c_s$ . Denoting the dimensionless free energy density for the full model by  $f$ , I write

$$f(\phi, \phi_s) = f^{(0)}(\phi) + \phi_s[\log \phi_s - 1] + (Q\phi + \phi_s)[\log(Q\phi + \phi_s) - 1] \quad (1)$$

where the last two terms are the ideal mixing terms from the coions and counterions respectively, written using  $\phi_s \equiv V_p c_s$  for notational simplicity. Unimportant constants and terms linear in  $\phi$  or  $\phi_s$  have been dropped.

This free energy is a function of two density variables, namely  $\phi$  and  $\phi_s$ . A phase equilibrium such as between protein crystals and protein solution corresponds to equality of osmotic pressure and chemical potentials for *both* components. As a consequence there will in general be *different* values of  $\phi_s$  in coexisting phases, a salt partitioning effect which is not usually taken into account.

To solve for phase equilibria, it is useful to transform  $f$  into a semi-grand potential  $h(\phi, \phi_s^{(R)})$  where  $\phi_s^{(R)} \equiv V_p c_s^{(R)}$  is a dimensionless salt *reservoir* concentration [19]. To make this transformation note that the salt chemical potential is

$$\beta\mu_s = \frac{\partial f}{\partial \phi_s} = \log \phi_s + \log(Q\phi + \phi_s). \quad (2)$$

Now  $\phi_s \rightarrow \phi_s^{(R)}$  in the limit  $\phi \rightarrow 0$ , therefore  $\beta\mu_s = 2\log \phi_s^{(R)}$ . This gives

$$(\phi_s^{(R)})^2 = \phi_s(Q\phi + \phi_s) \quad (3)$$

which is the Donnan equilibrium result that the product of the coion and counterion concentrations takes a constant value in all phases including the reservoir. Solving this gives

$$\phi_s = [(Q^2\phi^2 + 4(\phi_s^{(R)})^2)^{1/2} - Q\phi]/2. \quad (4)$$

The semi-grand potential is  $h = f - \beta\mu_s\phi_s$  and the first two derivatives with respect to  $\phi$  at constant  $\phi_s^{(R)}$  (after a few lines of calculus) are

$$h = f^{(0)} + Q\phi \log(Q\phi + \phi_s) - (Q\phi + 2\phi_s), \quad (5)$$

$$\partial h / \partial \phi = \partial f^{(0)} / \partial \phi + Q \log(Q\phi + \phi_s), \quad (6)$$

$$\partial^2 h / \partial \phi^2 = \partial^2 f^{(0)} / \partial \phi^2 + Q^2 / (Q\phi + 2\phi_s). \quad (7)$$

The advantage of this transformation is that  $h$  is effectively a one-component free energy and can be treated accordingly. To use these results, one should remember to substitute for  $\phi_s$  from Eq. (4). For example, the osmotic pressure follows from  $V_p \beta \Pi = \phi(\partial h / \partial \phi) - h$ , ie

$$\Pi = \Pi^{(0)} + kT(Qc_p + 2c_s). \quad (8)$$

This shows explicitly the small ions behaving ideally, at a total concentration  $Qc_p + 2c_s$ .

What is obvious from these results is that there is a cross-over in behaviour at  $Qc_p \sim c_s$  or salt concentrations of the order  $Q\phi/V_p$ . The *difference* in protein volume fraction between the solution and crystal is often  $\Delta\phi \sim 0.5$ . Putting  $Q \sim 10$ , and  $V_p \sim 10 \text{ M}^{-1}$ , this corresponds to a cross-over salt concentration  $\sim 0.5 \text{ M}$ . If the salt concentration is much less than this, there will be a

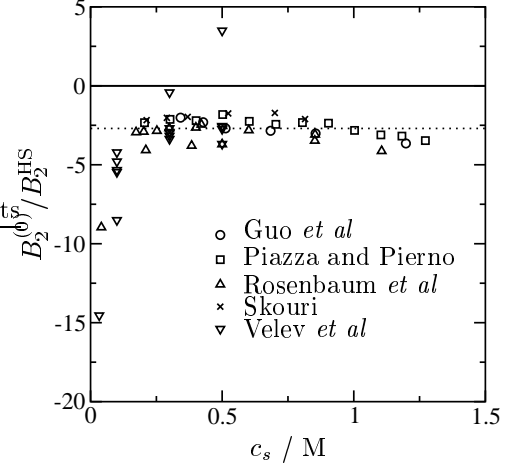


FIG. 1:  $B_2^{(0)}/B_2^{\text{HS}}$  for lysozyme [12, 20], as a function of  $c_s$ , where  $B_2^{(0)} = B_2 - Q^2/4c_s$ . The dashed line is the average, Eq. (10), for all data with  $c_s > 0.25 \text{ M}$ . The ‘rogue’ point from Velev *et al* with  $B_2^{(0)} > 0$  is for  $Q = 3.6$ .

large osmotic pressure difference between the crystal and the solution due to the counterions, having the effect of narrowing the coexistence gap. This is the basic reason why the coexistence boundary occurs at salt concentrations of this order of magnitude in this model. It is a much larger cross-over salt concentration than intuition might have suggested based on experiences for colloidal systems (eg  $Q \sim 10^3$ ,  $V_p \sim 10^6 \text{ nm}^3$  gives  $c_s \sim 10^{-3} \text{ M}$ ), but then globular proteins are much smaller than colloids.

On the other hand, typical protein solutions on the crystallisation boundary have  $\phi \sim 0.05$ , corresponding to a cross-over salt concentration  $\sim 50 \text{ mM}$ . For salt concentrations much larger than this, the free energy contribution from the small ions is essentially dominated by a term  $Q^2\phi^2/4\phi_s$  (from Eq. (7) and noting that constants and terms linear in  $\phi$  are unimportant). The effects of salt and charge are subsumed into a scaling variable  $\phi_s/Q^2$  and this is the basic reason for the scaling of both the crystallisation boundary and  $B_2$ . In the remaining sections, I place these arguments on a firm footing, starting with a discussion on the second virial coefficient since this is not dependent on any particular baseline model.

### III. SECOND VIRIAL COEFFICIENT

The prediction of the present theory for  $B_2$  can be obtained from the osmotic pressure result Eq. (8) (recalling that Eq. (4) should be used for  $\phi_s$ ), or directly by inspection from Eq. (7). Either way

$$B_2 = B_2^{(0)} + Q^2/4c_s. \quad (9)$$

One can also show the same result is obtained for light scattering, since charge density fluctuations are sup-

pressed in the long wavelength limit. Thus if the present approach is correct, the effects of charge and salt should be confined to the second term in Eq. (9): is there any evidence this is so? Egelhaaf and Poon have collected experimental data on  $B_2$  from the available literature [12, 20]. This data is used to construct Fig. 1 which shows  $B_2 - Q^2/4c_s$ , normalised by the value expected if lysozyme proteins behaved as hard spheres, namely  $B_2^{\text{HS}} = 4V_p \approx 85 \text{ nm}^3$  (this is close to  $B_2^{\text{HS}} = 82.3 \text{ nm}^3$  used in [21]). Inspecting Fig. 1, it appears there is indeed a plateau for  $c_s \gtrsim 0.25 \text{ M}$  in agreement with Eq. (9), although perhaps a slight downwards trend can be detected at high salt and there may also be a problem if the protein charge is too small. There is considerable variation in the data, even for measurements at supposedly identical state points, which reflects the experimental difficulties in obtaining  $B_2$ . Averaging over all results in the plateau region in Fig. 1 arrives at

$$B_2^{(0)} \approx (-2.7 \pm 0.2) \times B_2^{\text{HS}}. \quad (10)$$

This result will be used to tie down the subsequent models for the crystallisation phase boundary.

#### IV. SEAR'S MODEL

To apply the general formalism to the prediction of crystallisation boundaries, one needs a well defined baseline model. Such a model should encompass both the fluid and crystal phases, and have a second virial coefficient consistent with the analysis above. A suitable model has been devised by Sear [8].

Sear's model comprises hard spheres (HS) with 'sticky patches'. The HS diameter is  $\sigma$ , chosen such that  $\pi\sigma^3/6 = V_p$  (ie  $\sigma \approx 3.4 \text{ nm}$ ). There are  $n_s$  sticky patches per sphere which associate in pairs and are characterised by a range  $r_c$ , an angular width  $\theta_c$ , and a depth  $\epsilon$ . The free energy of the fluid (F) phase (I reproduce only the essential details of the model here) is

$$f_F^{(0)}(\phi) = f_{\text{HS}}(\phi) + \phi n_s [\log p + (1-p)/2]. \quad (11)$$

In this  $f_{\text{HS}}$  is the HS fluid free energy and  $p$  is the proportion of non-bonded sites, solving  $(1-p)/p^2 = k\phi g_{\text{HS}}$  where

$$k = 6(r_c/\sigma - 1)(1 - \cos\theta_c)^2 e^{\beta\epsilon} \quad (12)$$

is a dimensionless bond association constant. The association equilibrium includes an enhancement factor,  $g_{\text{HS}}$ , for the HS pair correlation function at contact. The second virial coefficient in this model is given by

$$B_2^{(0)} = B_2^{\text{HS}} - (n_s/2) k V_p. \quad (13)$$

It is apparent that the fluid phase properties are completely determined by  $k$  and  $n_s$ . The model predicts fluid-fluid phase separation for sufficiently large values

TABLE I: Critical points for Sear's model showing critical volume fraction  $\phi^{(\text{C})}$ , dimensionless association equilibrium constant  $k^{(\text{C})}$ , and second virial coefficient  $B_2^{(\text{C})}$ .

$n_s$	$\phi^{(\text{C})}$	$k^{(\text{C})}$	$B_2^{(\text{C})}/B_2^{\text{HS}}$
4	0.09	16.8	-7.38
5	0.12	7.02	-3.39
6	0.15	3.90	-1.93
8	0.21	1.77	-0.77

of  $k$ , and table I gives the critical point for  $n_s = 4-8$ . Note that  $B_2^{(\text{C})}$  in this model provides an interesting counterexample to the observation of Vliegenthart and Lekkerkerker that  $B_2^{(\text{C})}/B_2^{\text{HS}} \approx -1.5$  for a wide variety of other models [22]. Whether fluid-fluid phase separation is metastable in this model depends on the actual values of  $r_c$ ,  $\theta_c$  and  $\beta\epsilon$ , and examples of both are given by Sear.

Sear provides a cell model for the protein chemical potential in an ordered cubic phase, arguing that osmotic pressure is not important. My approach here is slightly different. I use the same cell model to specify the free energy and take into account the osmotic pressure. The results are not essentially different from Sear's results, although the analysis does point up an important property of Sear's model (Fig. 2 below). Following Sear, the free energy per protein in the crystal (X) is

$$f_X^{(0)}(\phi)/\phi = C - 3 \log(a/\sigma - 1) - \log(\theta_c^3/\pi^2) - (n_s/2) \beta\epsilon w[(\phi - \phi_{\min})/\delta\phi] \quad (14)$$

where  $a/\sigma = (6\phi/\pi)^{-1/3}$  is the unit cell size relative to the HS diameter. The constant in this is  $C = \log(V_p/\sigma^3)$ , provided that  $f_{\text{HS}} \sim \phi(\log\phi - 1)$  in the fluid phase as  $\phi \rightarrow 0$ . This free energy is appropriate for  $\phi \gtrsim \phi_{\min}$  where  $\phi_{\min} = \pi(\sigma/r_c)^3/6$  is the volume fraction around which the bonds in the crystal become dissociated. As  $\phi$  decreases past  $\phi_{\min}$  the last term in Eq. (14) vanishes rapidly. To implement this I have introduced an *ad hoc* cut-off function  $w[(\phi - \phi_{\min})/\delta\phi]$  in the last term, where  $\delta\phi$  sets the rate at which the cut-off operates. For the present calculations I take  $w[x] = 1/(1 + e^{-x})$  and  $\delta\phi = 0.01$ . This cut-off function represents the way in which the short-range attraction potential falls off with distance in the model. The actual details may shift the phase boundaries but are not important for the broad picture.

Although several values of the parameters in the model were examined, I only report in detail here on calculations for  $n_s = 6$ ,  $r_c = 1.05\sigma$  and  $\theta_c = 0.45$  (so the range of the attraction is  $r_c - \sigma \approx 2 \text{ \AA}$  and the angular width about  $26^\circ$ ). These values give quite good agreement with the crystallisation boundaries for lysozyme. Following a rather different analysis of a model similar to Sear's model, Curtis *et al* also conclude  $n_s = 6-8$  is appropriate [23].

Fig. 2 shows the fluid and crystal free energies for  $n_s = 6$ ,  $r_c = 1.05\sigma$  and  $\theta_c = 0.45$ , for two values of  $\beta\epsilon$ . It is

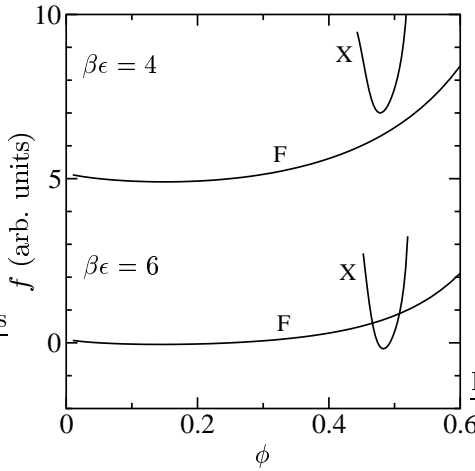


FIG. 2: Free energy for Sear's model ( $n_s = 6$ ,  $r_c = 1.05\sigma$ ,  $\theta_c = 0.45$ ) illustrating metastability of crystal branch (X) with respect to fluid branch (F) for  $\beta\epsilon \lesssim 4.8$ .

clear that there is a certain minimum value  $\beta\epsilon \approx 4.8$  below which the crystal is *metastable* with respect to the fluid. This is an important contrast with the AHS model (next section) in which the ordered phase is present at  $\beta\epsilon \rightarrow 0$ . Crystallisation in Sear's model is essentially an *energetic* transition to an ordered phase dominated by the directional interactions (compare ‘energetic fluid’ concept introduced by Louis [24]), and not a continuation of the *entropic* HS freezing transition. The position of the sticky patches controls the crystal structure, and as suggested by Sear, this may explain the relative ease or difficulty of crystallising various proteins. In this context, note that lysozyme forms tetragonal crystals with well-aligned molecules (otherwise X-ray diffraction would be useless) at a volume fraction around 0.5—it is difficult to attribute all this solely to packing considerations!

Fig 3 shows the phase behaviour for the model for the chosen parameter set. The solid lines in Fig 3 are for the baseline model. As  $\beta\epsilon$  increases, the fluid-crystal phase transition widens (the re-entrant fluid phase expected at larger  $\phi$  is not shown). There is a metastable fluid-fluid phase separation for  $\beta\epsilon \gtrsim 7.18$ .

The effect of charges and added salt is obtained by inserting the baseline model into the general formalism in section II. The dashed line in Fig. 3 shows the fluid-crystal phase boundary at  $Q = 10$  in the absence of salt. The transition has been markedly narrowed and the fluid-fluid transition moves to such a high value of  $\beta\epsilon$  that it is no longer on the diagram. Repeating the calculation for  $c_s^{(R)} = 0.2 \text{ M}$  obtains the chained lines in Fig. 3. The fluid-crystal phase boundary is intermediate between the zero salt limit and the baseline model, and the metastable fluid-fluid transition has reappeared in the diagram for  $\beta\epsilon \gtrsim 9.14$ . Finally as  $c_s^{(R)} \rightarrow \infty$ , the phase boundaries all move back to coincide with the baseline model. Thus

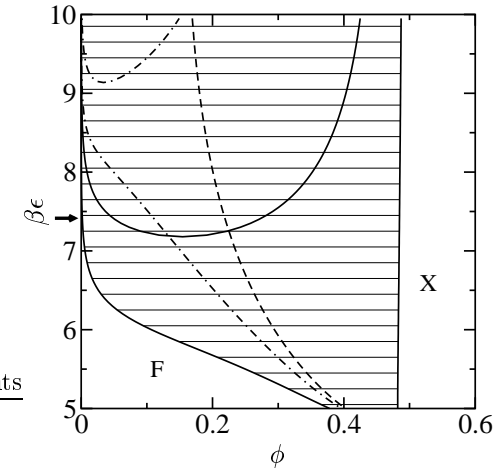


FIG. 3: Phase behaviour in  $(\phi, \beta\epsilon)$  plane for Sear's model ( $n_s = 6$ ,  $r_c = 1.05\sigma$ ,  $\theta_c = 0.45$ ): solid lines are for the baseline model ( $Q = c_s^{(R)} = 0$ ), dashed line is for  $Q = 10$  and  $c_s^{(R)} = 0$ , and chained lines are for  $Q = 10$  and  $c_s^{(R)} = 0.2 \text{ M}$ .

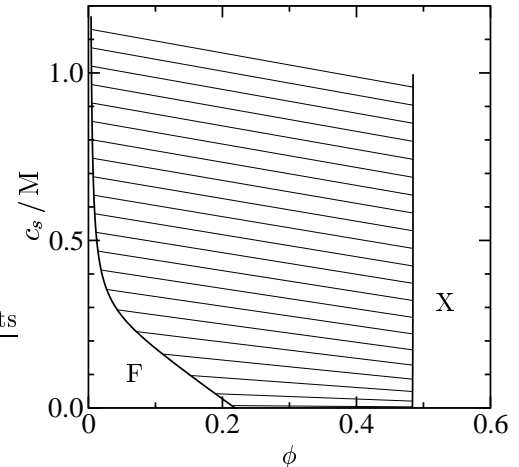


FIG. 4: Phase behaviour in  $(\phi, c_s)$  plane for Sear's model ( $n_s = 6$ ,  $r_c = 1.05\sigma$ ,  $\theta_c = 0.45$ ,  $\beta\epsilon = 7.4$ ) for  $Q = 10$ .

the effect of charge in the model is to strongly suppress existing phase transitions in the absence of added salt. This is because of the big contribution the counterions make to the osmotic pressure. Adding salt weakens and eventually destroys the effect. The salt concentration required to do this is  $c_s \sim Qc_p$ , as discussed already in section II.

I now set  $\beta\epsilon = 7.4$ , marked by an arrow in Fig. 3, so that  $B_2^{(0)}/B_2^{\text{HS}} = -2.7$  reproduces the value calculated in section III above. Fig 4 shows a typical phase diagram for the full model at this value of  $\beta\epsilon$ , as a function of added salt. Salt reservoir concentrations have been converted

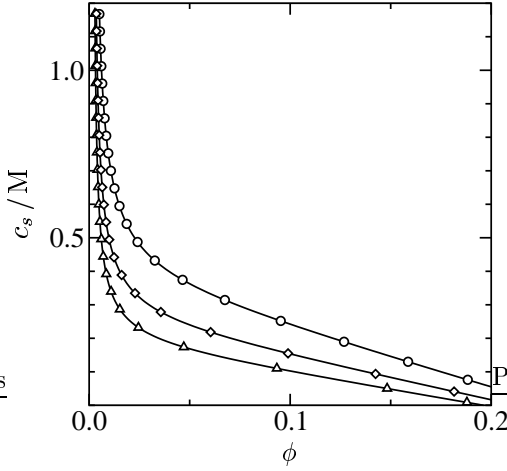


FIG. 5: Fluid-crystal binodals in  $(\phi, c_s)$  plane for Sear's model ( $n_s = 6$ ,  $r_c = 1.05\sigma$ ,  $\theta_c = 0.45$ ,  $\beta\epsilon = 7.4$ ) for  $Q = 8.0$  (triangles),  $9.4$  (diamonds) and  $11.4$  (circles).

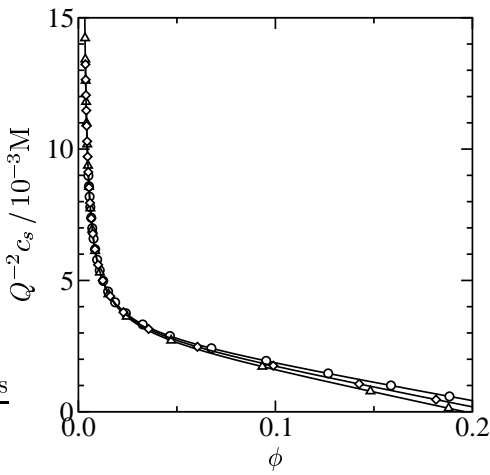


FIG. 6: Same data as Fig. 5 replotted in  $(\phi, Q^{-2} c_s)$  plane.

back to actual salt concentrations. The sloping tie-lines indicate a salt partitioning effect in which the coion concentration is enhanced in the more dilute phases. In this simple model I have not taken into account excluded volume in the dense phases, so in reality the salt partitioning would be more marked (see below for a further discussion on this). In this representation we can clearly see how adding salt broadens the fluid-crystal coexistence. Metastable fluid-fluid phase separation does not appear until salt concentrations  $\gtrsim 2.3$  M for this value of  $\beta\epsilon$ .

This calculation is now repeated for  $Q = 8.0$ ,  $9.4$  and  $11.4$ , which are the three values of lysozyme charge examined experimentally by Poon *et al.* Fig. 5 shows the crystallisation boundary (ie fluid-crystal binodal) as a function of added salt. Clearly, the higher the charge, the

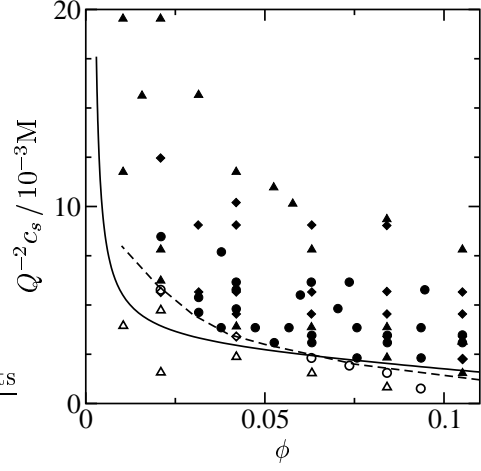


FIG. 7: Data on lysozyme crystallisation from the experiments of Poon *et al* [9], for  $Q = 8.0$  (triangles),  $9.4$  (diamonds) and  $11.4$  (circles). Filled (open) symbols indicate the occurrence (non-occurrence) of crystals. The dashed line is the approximate experimental crystallisation boundary. The solid line as the mean crystallisation boundary from Fig. 6.

more the phase transition is suppressed. Finally, these same phase boundaries are replotted in Fig. 6 as a function of the scaling variable  $c_s/Q^2$ . In this representation, the curves all collapse to lie on approximately the same quasi-universal crystallisation boundary. The scaling collapse is robust: if the calculations are repeated for different parameter values, the quasi-universal crystallisation curve moves up or down but a similar scaling collapse is always obtained.

The mean crystallisation boundary from Fig. 6 is shown in Fig 7, which now includes the experimental data from Poon *et al*. There is reasonable agreement on the location of the quasi-universal crystallisation boundary, although it appears there is always some discrepancy between the shape of the theoretical and experimental boundaries at low  $\phi$ . It is worth re-emphasising that the present model is constrained to have the correct  $B_2$ , at least for  $c_s \gtrsim 0.25$  M. The absence of a metastable fluid-fluid phase separation agrees with Poon *et al* who observe that no such phase transition occurs at the temperature of the experiments ( $22.5$  °C). However, a temperature decrease of just a few percent in the model, so that  $\beta\epsilon = 7.7$  for example, is sufficient to bring fluid-fluid phase separation to accessible salt concentrations in the range  $0.5$ – $1.0$  M. This is in accordance with the observations of Muschol and Rosenberger [25] (but caution is required since it is unlikely the only effect of temperature is through the value of  $\beta\epsilon$ ). In the scaling representation of Fig. 6 such metastable fluid-fluid binodals also collapse to a quasi-universal curve—this is a prediction of the theory that would be interesting to test experimentally.

Fig. 6 encompasses the central result for this paper.

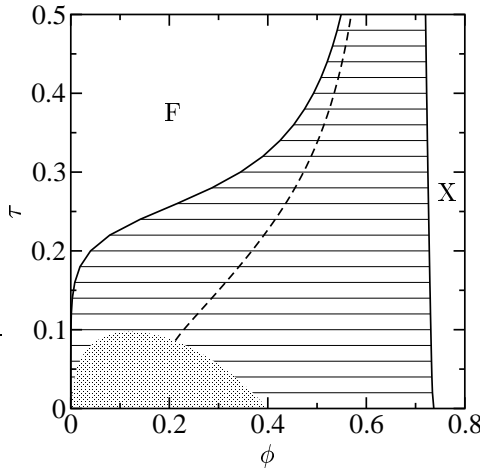


FIG. 8: Phase behaviour in  $(\phi, \tau)$  plane for the adhesive hard sphere model ( $n = 30$ ): solid lines are for baseline model ( $Q = c_s^{(R)} = 0$ ), dashed line is for  $Q = 10$  and  $c_s^{(R)} = 0$ . The shaded region is the ‘danger zone’, Eq. (17), for Baxter’s theory.

As discussed above, the scaling collapse occurs because the effects of charge and salt in fluid free energy are effectively combined into a single scaling variable  $c_s/Q^2$ , at salt concentrations in the vicinity of the crystallisation boundary. To show this is not just a feature of Sear’s model, I now turn briefly to the more commonly studied AHS model.

## V. ADHESIVE HARD SPHERE MODEL

The adhesive hard sphere (AHS) model is also a suitable baseline model for the general theory in section II. In this model, hard spheres interact with a short range isotropic attractive potential. As noted by Rosenbaum *et al* [4], the phase behaviour is largely insensitive to the details of the potential provided the second virial coefficient is used as the effective temperature axis. My approach to the baseline model here is closely based on that of Noro *et al* who investigated the effects of long range forces on the AHS model [26].

For the fluid phase, I use Barboy’s treatment of Baxter’s analytic theory [27]. In Baxter’s theory [28], the attractive potential is characterised by a ‘stickiness’ parameter  $\tau$  which is related to the second virial coefficient by

$$B_2^{(0)}/B_2^{\text{HS}} = 1 - (4\tau)^{-1}. \quad (15)$$

The crystal phase is expected to be FCC since this has the greatest density of intersphere contacts. As the stickiness is switched off ( $\tau \rightarrow \infty$  or  $\beta\epsilon \rightarrow 0$ ) the fluid-crystal phase transition goes over into the usual HS freezing transition, which is a contrast to Sear’s model. The

AHS ordered phase has always proved rather more difficult to treat analytically than the fluid phase, and approaches have ranged through density functional calculations by Marr and Gast [5], and Tejero and Baus [6], to detailed simulation studies of a particular realisation of the AHS model by Hagen and Frenkel [7]. Here I use the cell model of Daanoun *et al* for the crystal phase free energy [29], assuming the attractive part of the AHS potential is  $-\epsilon(r/\sigma)^{-n}$  with  $n \gg 1$ . The cell model free energy is almost identical to that already used in Eq. (14) with  $n_s = 12$  for the FCC structure. The difference is that there is no restriction on orientation so the term  $-\log(\theta_c^3/\pi^2)$  is absent, and the role played by the *ad hoc* cut-off function is taken over by the functional form of the actual short range potential, ie  $w[x] \rightarrow (a/\sigma)^{-n}$ . Like the choices for the cut-off function in the previous section, the actual value of  $n$  may shift the phase boundaries but doesn’t change the broad picture. For the purposes of the present calculation I set  $n = 30$ .

A link between the cell model for the crystal phase and the Baxter-Barboy treatment of the fluid phase can be made by matching  $B_2$  of Eq. (15) with the exact expression

$$B_2^{(0)}/B_2^{\text{HS}} = 1 + 3 \int_1^\infty dx x^2 [1 - \exp(-\beta\epsilon x^{-n})]. \quad (16)$$

Fig. 8 shows the phase behaviour for the model. The solid line in this figure is the fluid-crystal phase boundary for the baseline model, and the dashed line is the corresponding boundary for  $Q = 10$  with no salt. Similar to Fig. 3, the effect of charge is to narrow the fluid-crystal transition. As salt is added (not shown here), the boundary moves back towards that of the baseline model.

There is a complication that arises for Baxter’s solution for the AHS fluid phase free energy. Baxter’s theory involves the solution of a quadratic equation. If

$$\tau < \frac{(12\phi + 6\phi^2)^{1/2} - 6\phi}{6(1 - \phi)} \quad (17)$$

then this quadratic equation has complex roots and Baxter’s theory becomes inadmissible. Normally this ‘danger zone’, shown shaded in Fig. 8, is happily hidden within the fluid-crystal two phase region. In the charged version though, it emerges into the single phase fluid region. For this reason one cannot choose  $\tau < (2 - \sqrt{2})/6 \approx 0.098$ , the maximum of Eq. (17), and unfortunately this excludes  $\tau = 0.067$  which would match  $B_2^{(0)}/B_2^{\text{HS}} = -2.7$  from section III.

To demonstrate the scaling collapse for this model, I therefore choose  $\tau = 0.1$  (equivalent to  $B_2^{(0)}/B_2^{\text{HS}} = -1.5$  [22]). I repeat the calculations of the previous section to obtain the crystallisation boundaries (fluid-crystal binodal) as a function of added salt, for  $Q = 8.0, 9.4$  and  $11.4$  as used previously. Fig. 9 shows these boundaries plotted using the scaling variable  $c_s/Q^2$ . Again the curves collapse to a quasi-universal crystallisation boundary, similar to those in Fig. 6. This result confirms that the scaling collapse is a common feature for two different baseline models for the phase behaviour.

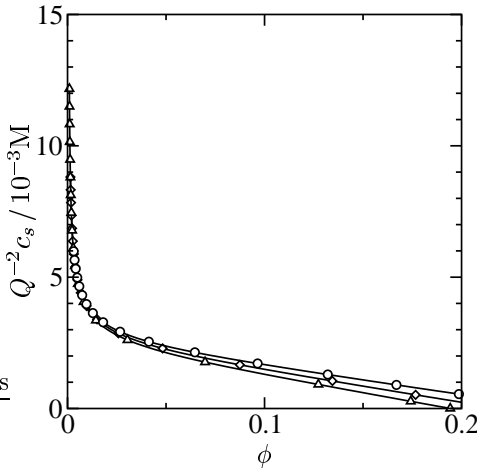


FIG. 9: Fluid-crystal binodals in  $(\phi, Q^{-2} c_s)$  plane for the adhesive hard sphere model ( $n = 30$ ,  $\tau = 0.1$ ) for  $Q = 8.0$  (triangles), 9.4 (diamonds) and 11.4 (circles).

## VI. DONNAN EQUILIBRIUM

If the general theory in section II is to be taken seriously, then there are some interesting physical implications for the equilibrium between crystals and solution which are explored in this section.

The first implication concerns salt partitioning. In the simple theory of section II, the product of coion and counterion concentrations is a constant as in Eq. (3). Each phase has to be electrically neutral, so that a phase enriched in protein is also enriched in counterions, and consequently *depleted* in coions (Donnan common ion effect). This explains the slope of the tie-lines in Fig. 4 for example. We can ask: is there any independent evidence for this phenomenon?

Let me preface the answer to this by some cautionary remarks. Deviations from the simple Donnan equilibrium result may arise from three sources. Firstly excluded volume effects mean one should really consider the small ion concentrations in the available free volume. This will be an important consideration in the crystal phase where the volume fraction occupied by the protein is  $\sim 50\%$ . Secondly, deviations from ideal solution behaviour can be expected at high salt concentrations—such deviations are usually absorbed into ‘activity coefficients’. Thirdly there may be significant specific ion effects, such as seen in the Hoffmeister series.

The evidence in support of salt partitioning comes from recent experiments by Morozova *et al* on cross-linked lysozyme crystals in contact with salt solutions [30]. For example, table II shows concentrations of  $\text{Na}^+$  and  $\text{Cl}^-$  in solution and in the crystal. There is marked partitioning: the coion concentration in the crystal free volume is about half that in the external solution. The product of the two ion concentrations is approximately constant

TABLE II: Lysozyme salt partitioning data from Palmer *et al* [31], cited in Morozova *et al* [30]. Solution is 0.855 M  $\text{NaCl}$  / 0.2 M  $\text{NaAc}$  buffer ( $pH = 4.5$ ). Ion concentrations in the third column are calculated by multiplying those in the second column by  $1/(1 - \phi)$ , where  $\phi = 0.64$  is the crystal volume fraction. The charge unaccounted for in the crystal, assuming  $Q = 11.4$ , is 0.05 M or  $\sim 3\%$  of the total charge.

conc / M	solution	crystal	crystal free volume
$\text{Lysozyme}^{Q+}$		0.056	
$\text{Ac}^-$	0.2		
$\text{Na}^+$	1.055	0.19	0.53
$\text{Cl}^-$	0.855	0.78	2.2
$\text{Na}^+ \times \text{Cl}^-$	0.9		1.2

(final row in Table II), provided the protein excluded volume is taken into account. More detailed calculations also taking into account activity coefficients give excellent agreement between the theory and experimental results [30], and Morozova *et al* conclude “... for small ions capable of penetrating into the crystal channels [the] electrostatic (Donnan) potential controls the equilibrium internal concentration of ions in just the same way as in polyelectrolyte gels.”

By way of contrast, the same work also suggests  $\text{Br}^-$  has a significant specific interaction with lysozyme. In the context of the present paper, this would suggest there should be a significant deviation away from the quasi-universal crystallisation boundary if  $\text{NaBr}$  is used instead of  $\text{NaCl}$ .

The second implication concerns the electrical structure of the interface between crystal and solution phases. In the Donnan membrane equilibrium [13, 14], an electrostatic potential difference develops between the two compartments on either side of the membrane. This is known as a *Donnan potential*. In the present theory for protein crystallisation, it is still true that a difference in the mean electrostatic potential develops between the crystals and the solution phase. Whether this should also be called a Donnan potential, a *Galvani potential*, or perhaps something else, can be debated [32].

At any rate, the potential difference is readily calculated given the salt partitioning (see Appendix for more details). If  $c_+$  and  $c_-$  are the coion and counterion concentrations respectively, then Eq. (A13) in the Appendix translates to

$$c_{\pm} = c_s^{(\text{R})} \exp[\mp \beta e \bar{\varphi}], \quad (18)$$

where  $\bar{\varphi}$  is the mean electrostatic potential in the phase of interest measured relative to the salt reservoir (this result can also be used to recover Eq. (3)). The difference in mean potential between fluid (F) and crystal (X) phases,  $\Delta\varphi = \bar{\varphi}^{(\text{X})} - \bar{\varphi}^{(\text{F})}$ , is

$$\Delta\varphi = (\beta e)^{-1} \log(c_s^{(\text{F})}/c_s^{(\text{X})}). \quad (19)$$

For example, for the salt concentrations in Table II,  $c_s^{(\text{F})} = 1.055 \text{ M}$ ,  $c_s^{(\text{X})} = 0.53 \text{ M}$  (in the free volume), and

therefore  $\Delta\varphi \approx 17$  mV. The potential difference arises because an electrical double layer is formed at the crystal-solution interface and is intimately connected with salt partitioning. Pair-potential theories miss these effects, which are essentially many-body phenomena. I have discussed this in more detail in the context of charged colloidal systems [33].

## VII. CONCLUSIONS

There are two major conclusions from the present work. The first is specific to lysozyme, and the second more generally concerns the role of electrostatic effects and the use of effective pair potentials for protein phase equilibria.

Firstly, the lysozyme system does appear to be well characterised by the present theory. The quasi-universal crystallisation boundary can be fit reasonable well by the present version of Sear's model with  $\sim 6$  sticky contacts per molecule. The scaling collapse for  $B_2$  noticed by Egelhaaf and Poon is here attributed to a Donnan contribution  $Q^2/4c_s$  added to a 'bare'  $B_2^{(0)}$  which is approximately *independent* of salt concentration above about 0.25 M. The scaling collapse for the crystallisation boundaries can similarly be attributed a Donnan effect. In this system therefore, NaCl appears to be acting as an *indifferent electrolyte* in the sense that it obeys the rules for Donnan equilibrium reasonably well and does not seem to exhibit specific ion effects. This appears to be confirmed by the experiments of Morozova *et al* discussed in the preceeding section.

The second conclusion concerns the importance of the electrostatic effects in protein crystallisation. The twin phenomena of salt partitioning and the appearance of a significant Donnan potential difference  $\Delta\varphi$  go hand-in-hand. These are essentially many-body effects, and are not captured in simple pair-potential theories. This conclusion mirrors Langmuir's critique of the use of pair potentials for colloidal equilibrium [34]. The importance of these effects is measured by the magnitude of  $\Delta\varphi$  relative to thermal energy  $kT$ . If  $\Delta\varphi \gtrsim kT/e$  then there may be significant errors introduced by using a single effective pair potential (such as a DLVO potential) for both the crystal and the solution phases. On the other hand, if  $\Delta\varphi \ll kT/e$ , the use of pair potentials cannot be criticised on these grounds. It can easily be shown that  $\Delta\varphi \gtrsim kT/e$  corresponds to salt concentrations smaller than the protein charge density in the crystal, typically 0.5 M. Salt concentrations smaller than this are often encountered, and so the above effects may often be important.

## VIII. ACKNOWLEDGMENTS

I thank W. C. K. Poon and S. U. Egelhaaf for many discussions and for sharing data on  $B_2$ , M. G. Noro for

discussions on the AHS model, H. N. W. Lekkerkerker for drawing my attention to Hill's papers, and M. E. Fisher for discussions on the Donnan potential in phase equilibria.

## APPENDIX A: DERIVATIONS FROM POISSON-BOLTZMANN THEORY

I wish to discuss the relationship between Poisson-Boltzmann theory, the Debye-Hückel approximation and the Donnan approach in the main text. The discussion will be largely pedagogical since similar results are obtained for more specific problems by von Grünberg *et al* [35], van Roij *et al* [36], amongst others [16, 33].

To approach this systematically requires a common starting point. I will choose this to be a general expression for the grand potential for univalent small ions at densities  $\rho_{\pm}(\mathbf{r})$ , in the presence of external charge density  $\rho_{\text{ext}}(\mathbf{r})$ . For simplicity, I will drop excluded volume effects and other interactions. If the external charge density is due to protein molecules for instance, this grand potential provides the many-body potential of mean force for the proteins in precisely the sense of McMillan-Mayer theory [15, 16]. The grand potential is

$$\Omega = \Omega_{\text{id}} + \Omega_{\text{mf}} + \Omega_{\text{ex}}. \quad (\text{A1})$$

In this, the ideal contribution is

$$\beta\Omega_{\text{id}} = \int d^3\mathbf{r} \sum_{\alpha=\pm} \rho_{\alpha}(\mathbf{r}) \left[ \log \frac{\rho_{\alpha}(\mathbf{r})}{\rho_s} - 1 \right]. \quad (\text{A2})$$

There has to be the same chemical potential  $\mu_s$  for both species and I have incorporated  $\rho_s \equiv e^{\beta\mu_s}$  into the ideal term. The mean field electrostatic term is

$$\beta\Omega_{\text{mf}} = \frac{l_B}{2} \int d^3\mathbf{r} d^3\mathbf{r}' \frac{\rho_Q(\mathbf{r})\rho_Q(\mathbf{r}')}{|\mathbf{r} - \mathbf{r}'|} \quad (\text{A3})$$

where

$$\rho_Q(\mathbf{r}) = \rho_+(\mathbf{r}) - \rho_-(\mathbf{r}) + \rho_{\text{ext}}(\mathbf{r}) \quad (\text{A4})$$

is the total charge density. Finally  $\Omega_{\text{ex}}$  captures correlation effects beyond mean field electrostatics.

If we define

$$\varphi(\mathbf{r}) = l_B \int d^3\mathbf{r}' \frac{\rho_Q(\mathbf{r}')}{|\mathbf{r} - \mathbf{r}'|} \quad (\text{A5})$$

as a dimensionless electrostatic potential, then  $\varphi$  obeys the Poisson equation,

$$\nabla^2 \varphi + 4\pi l_B \rho_Q = 0. \quad (\text{A6})$$

Poisson-Boltzmann theory amounts to the neglect of correlations beyond the mean field term. To show this, set

$\Omega_{\text{ex}} = 0$ , then the variational minimum  $\delta\Omega/\delta\rho_{\pm}(\mathbf{r}) = 0$  solves to

$$\rho_{\pm}(\mathbf{r}) = \rho_s e^{\mp\varphi(\mathbf{r})}. \quad (\text{A7})$$

Inserting into Eq. (A6) gives the Poisson-Boltzmann equation

$$\nabla^2\varphi - \kappa_s^2 \sinh \varphi + 4\pi l_B \rho_{\text{ext}} = 0 \quad (\text{A8})$$

where  $\kappa_s^2 = 8\pi l_B \rho_s$ . From Eqs. (A7) and (A1)–(A3) it is easy to show that

$$\beta\Omega = \int d^3\mathbf{r} \left( \frac{1}{2} \varphi \rho_{\text{ext}} + \rho_s (\varphi \sinh \varphi - 2 \cosh \varphi) \right). \quad (\text{A9})$$

Thus to summarise, the Poisson-Boltzmann equation, Eq. (A8), should be solved for  $\varphi$ , then Eq. (A9) gives the Poisson-Boltzmann free energy associated with the external charge density. This free energy is a non-linear functional of  $\rho_{\text{ext}}(\mathbf{r})$  and can be used as a many-body potential of mean force between the elements comprising the external charge density.

Now I consider two further approximations. To regularise certain otherwise divergent integrals, I shall assume  $1/r \rightarrow e^{-\mu r}/r$  in the electrostatic energy integrals, where  $\mu > 0$  is a small inverse length taken to zero at the end of any calculations. However I shall not explicitly show this regularisation unless necessary.

The first approximation is very simple: set the small ion densities equal to constants independent of position, ie  $\rho_{\pm} = \bar{\rho}_{\pm}$ . Then

$$\frac{\beta\Omega_{\text{id}}}{V} = \sum_{\alpha=\pm} \bar{\rho}_{\alpha} \left[ \log \frac{\bar{\rho}_{\alpha}}{\rho_s} - 1 \right], \quad (\text{A10})$$

and making use of the above regularisation

$$\frac{\beta\Omega_{\text{mf}}}{V} = \frac{2\pi l_B}{\mu^2} \bar{\rho}_Q^2 + \frac{l_B}{2V} \int d^3\mathbf{r} d^3\mathbf{r}' \frac{\Delta\rho_{\text{ext}}(\mathbf{r}) \Delta\rho_{\text{ext}}(\mathbf{r}')}{|\mathbf{r} - \mathbf{r}'|} \quad (\text{A11})$$

where  $\bar{\rho}_Q = \bar{\rho}_+ - \bar{\rho}_- + \bar{\rho}_{\text{ext}}$ ,  $\bar{\rho}_{\text{ext}} = (1/V) \int d^3\mathbf{r} \rho_{\text{ext}}(\mathbf{r})$ , and  $\Delta\rho_{\text{ext}}(\mathbf{r}) = \rho_{\text{ext}}(\mathbf{r}) - \bar{\rho}_{\text{ext}}$ .

The variational minimum,  $\partial\Omega/\partial\bar{\rho}_{\pm} = 0$ , gives

$$\log \frac{\bar{\rho}_{\pm}}{\rho_s} \pm \frac{4\pi l_B}{\mu^2} \bar{\rho}_Q = 0. \quad (\text{A12})$$

In the limit  $\mu \rightarrow 0$ , the solution to this pair of equations forces  $\bar{\rho}_Q \rightarrow 0$ . This happens in such a way that  $4\pi l_B \bar{\rho}_Q/\mu^2 \rightarrow \bar{\varphi}$ , the mean potential. To see this, explicitly write out the Poisson equation in its regularised form,  $\nabla^2\varphi - \mu^2\varphi + 4\pi l_B \rho_Q = 0$ . Integrate this over space, and assume that there are no electric fields at large distances, to get  $4\pi l_B \bar{\rho}_Q/\mu^2 = (1/V) \int d^3\mathbf{r} \varphi = \bar{\varphi}$  as promised. Eq. (A12) becomes

$$\bar{\rho}_{\pm} = \rho_s \exp[\mp\bar{\varphi}], \quad (\text{A13})$$

where the mean potential  $\bar{\varphi}$  is chosen in such a way that the charge neutrality condition  $\bar{\rho}_Q = 0$  is satisfied.

This result has already been invoked in the main text in Eq. (18) (note  $\bar{\varphi}$  is not dimensionless in the main text).

At the variational minimum, the grand potential is

$$\beta\Omega = \beta\Omega_{\text{id}}(\bar{\rho}_{\pm}) + \frac{l_B}{2} \int d^3\mathbf{r} d^3\mathbf{r}' \frac{\Delta\rho_{\text{ext}}(\mathbf{r}) \Delta\rho_{\text{ext}}(\mathbf{r}')}{|\mathbf{r} - \mathbf{r}'|}. \quad (\text{A14})$$

In other words it reduces to an ideal contribution from the small ion mean densities, and an electrostatic contribution from the deviation of the external charge density from the mean external charge density. Making the further mean field assumption that  $\rho_{\text{ext}} \rightarrow \bar{\rho}_{\text{ext}}$ , the last term vanishes too, and the Donnan method as used in the main text is recovered. If instead one uses Eq. (A14) for the potential of mean force, not only is there a direct electrostatic interaction, but an indirect many-body effect has crept in via the charge neutrality condition.

The second approximation elaborates this to recover Debye-Hückel theory. Write

$$\rho_{\pm}(\mathbf{r}) = \bar{\rho}_{\pm} + \Delta\rho_{\pm}(\mathbf{r}), \quad (\text{A15})$$

where  $\bar{\rho}_{\pm}$  are the mean densities given above. Expand  $\Omega_{\text{id}}$  to second order in  $\Delta\rho_{\pm}(\mathbf{r})$  and treat the resulting free energy as a variational problem for  $\Delta\rho_{\pm}(\mathbf{r})$ . The term  $\Omega_{\text{mf}}$  does not require approximation since it is already quadratic in  $\Delta\rho_{\pm}$ . Requiring  $\delta\Omega/\delta(\Delta\rho_{\pm}) = 0$  yields  $\Delta\rho_{\pm} = \mp\bar{\rho}_{\pm}(\varphi - \bar{\varphi})$  where  $\varphi$  satisfies the *original* Poisson equation, Eq. (A6). Note that since  $\bar{\varphi}$  is the mean potential, it follows that  $\int d^3\mathbf{r} \Delta\rho_{\pm} = 0$ , in other words, the interpretation of  $\bar{\rho}_{\pm}$  as mean values is correct. Inserting this result into the Poisson equation gives, after some rearrangement,

$$\nabla^2(\varphi - \bar{\varphi}) - \kappa^2(\varphi - \bar{\varphi}) + 4\pi l_B \Delta\rho_{\text{ext}} = 0 \quad (\text{A16})$$

where  $\kappa^2 = 4\pi l_B(\bar{\rho}_+ + \bar{\rho}_-) = 8\pi l_B \rho_s \cosh \bar{\varphi}$ . The solution to this linearised Poisson-Boltzmann equation is

$$\varphi(\mathbf{r}) = \bar{\varphi} + l_B \int d^3\mathbf{r}' \frac{e^{-\kappa|\mathbf{r}-\mathbf{r}'|}}{|\mathbf{r} - \mathbf{r}'|} \Delta\rho_{\text{ext}}(\mathbf{r}'). \quad (\text{A17})$$

On inserting these results into the grand potential, there are several cancellations and the final result is identical to Eq. (A14), apart from the unscreened Coulomb law being replaced by a screened Coulomb law with a screening length is given by  $\kappa^2 = 4\pi l_B(\bar{\rho}_+ + \bar{\rho}_-)$  where  $\bar{\rho}_{\pm} = \rho_s e^{\mp\bar{\varphi}}$ , and  $\bar{\varphi}$  is chosen to satisfy the electroneutrality condition  $\bar{\rho}_+ - \bar{\rho}_- + \bar{\rho}_{\text{ext}} = 0$ . Note that it is  $\Delta\rho_{\text{ext}}$  and not  $\rho_{\text{ext}}$  that appears in the electrostatic term once again, and if  $\rho_{\text{ext}} \rightarrow \bar{\rho}_{\text{ext}}$  only the ideal terms survive.

If we consider a limited system, such as a pair of colloid particles, then all average quantities are dominated by the bulk at large distances from the region of interest. In particular  $\bar{\varphi} \rightarrow 0$ ,  $\bar{\rho}_{\pm} \rightarrow \rho_s$ , and  $\kappa \rightarrow \kappa_s$ . In this way standard Debye-Hückel theory results are recovered.

This appendix has demonstrated that it is possible to recover Poisson-Boltzmann theory, the Donnan approach used in the main text, and a version of Debye-Hückel theory, starting systematically from the grand potential. All

approaches capture the many-body effects discussed in the conclusions in the main text. For Poisson-Boltzmann theory this is explicit. For the other approaches, it is

through the appearance of a mean electrostatic potential  $\bar{\varphi}$ , adjusted to take account of the charge neutrality condition.

---

[1] R. Piazza, *Curr. Opinion Coll. Int. Sci.* **5**, 38 (2000).

[2] W. C. K. Poon, *Phys. Rev. E* **55**, 3762 (1997).

[3] H. N. W. Lekkerkerker, *Physica A* **244**, 227 (1997).

[4] D. Rosenbaum, P. C. Zamora, and C. F. Zukowski, *Phys. Rev. Lett.* **76**, 150 (1996).

[5] D. W. Marr and A. P. Gast, *J. Chem. Phys.* **99**, 2024 (1993).

[6] C. F. Tejero and M. Baus, *Phys. Rev. E* **48**, 3793 (1993).

[7] M. H. J. Hagen and D. Frenkel, *J. Chem. Phys.* **101**, 4093 (1994).

[8] R. P. Sear, *J. Chem. Phys.* **111**, 4800 (1999).

[9] W. C. K. Poon, S. U. Egelhaaf, P. A. Beales, A. Salonen, and L. Sawyer, *J. Phys. Cond. Mat.* **12**, L569 (2000).

[10] C. Tanford and R. Roxby, *Biochem.* **11**, 2192 (1972).

[11] D. E. Kuehner, J. Engmann, F. Fergg, M. Wernick, H. W. Blanch, and J. M. Prausnitz, *J. Phys. Chem. B* **103**, 1368 (1999).

[12] S. U. Egelhaaf and W. C. K. Poon, private communications.

[13] F. G. Donnan, *Z. Elektrochem.* **17**, 572 (1911); F. G. Donnan and W. E. Garner, *Trans. Chem. Soc.* **115**, 1313 (1919); F. G. Donnan and E. A. Guggenheim, *Z. Physik. Chem.* **162**, 346 (1932); F. G. Donnan, *Z. Physik. Chem.* **168**, 369 (1934).

[14] Eg ch. 8 in *Polyelectrolyte solutions*, S. A. Rice and M. Nagasawa (Academic Press, London, 1961); ch. 7 in *Macromolecules in solution*, H. Morawetz (Wiley Interscience, New York, 1965).

[15] W. G. McMillan and J. E. Mayer, *J. Chem. Phys.* **13**, 276 (1945), for a recent review see [16].

[16] L. Belloni, *J. Phys. Cond. Mat.* **12**, R549 (2000).

[17] Perhaps the most important of these is T. L. Hill, *Disc. Faraday Soc.* **21**, 31 (1956); see also T. L. Hill, *J. Chem. Phys.* **22**, 1251 (1954); T. L. Hill, *J. Am. Chem. Soc.* **80**, 2923 (1958); D. Stigter and T. L. Hill, *J. Chem. Phys.* **63**, 551 (1959).

[18] M. L. Brodie, T. M. Tominc, and M. D. Saxowsky, *Phys. Rev. E* **53**, 6325 (1996).

[19] P. B. Warren, *J. Phys. II (France)* **7**, 343 (1997).

[20] Data is collected from B. Guo, S. Kao, H. McDonald, A. Asanov, L. L. Combs and W. W. Wilson, *J. Cryst. Growth* **196**, 424 (1999); R. Piazza and M. Pierno, *J. Phys. Cond. Mat.* **12**, A443 (2000); D. Rosenbaum *et al* from [21]; Skouri cited in Piazza and Pierno; O. D. Velev, E. W. Kaler and A. M. Lenhoff, *Biophys. J.* **75**, 2682 (1998).

[21] D. F. Rosenbaum, A. Kulkarni, S. Ramakrishnan, and C. F. Zukowski, *J. Chem. Phys.* **111**, 9822 (1999).

[22] G. A. Vliegenthart and H. N. W. Lekkerkerker, *J. Chem. Phys.* **112**, 5364 (2000).

[23] R. A. Curtis, H. W. Blanch, and J. M. Prausnitz, *J. Phys. Chem. B* **105**, 2445 (2001).

[24] A. A. Louis, *Phil. Trans. Roy. Soc. A* **359**, 939 (2001).

[25] M. Muschol and F. Rosenberger, *J. Chem. Phys.* **107**, 1953 (1997).

[26] M. G. Noro, N. Kern, and D. Frenkel, *Europhys. Lett.* **48**, 332 (1999).

[27] B. Barboy, *J. Chem. Phys.* **61**, 3194 (1974), note Barboy's definition of  $\tau$  differs from the present use and Baxter's original work by a factor 6.

[28] R. J. Baxter, *J. Chem. Phys.* **49**, 2770 (1968).

[29] A. Daanoun, C. F. Tejero, and M. Baus, *Phys. Rev. E* **50**, 2913 (1994).

[30] T. Y. Morozova, G. S. Kachalova, N. F. Lanina, V. U. Evtodienko, A. S. Botin, E. A. Shlyapnikova, and V. N. Morozov, *Biophys. Chem.* **60**, 1 (1996).

[31] K. J. Palmer, M. Ballantyne, and J. A. Galvin, *J. Am. Chem. Soc.* **70**, 906 (1948).

[32] M. E. Fisher, private communications; see also M. J. Sparnay, *The electrical double layer* (Pergamon, Oxford, 1972).

[33] P. B. Warren, *J. Chem. Phys.* **112**, 4683 (2000).

[34] I. Langmuir, *J. Chem. Phys.* **6**, 873 (1938), for an overview see [33].

[35] H. H. von Grünberg, R. van Roij, and G. Klein, *Europhys. Lett.* **55**, 580 (2001).

[36] R. van Roij, M. Dijkstra, and J.-P. Hansen, *Phys. Rev. E* **59**, 2010 (1999).